KLOE Note 206 October 2005

Search for $f_0(980)\to \pi^+\pi^-$ in $\pi^+\pi^-\gamma$ events with a photon at large angle

C.Bini, S.Ventura

Universitá "La Sapienza" and INFN Roma

Abstract

The selection of $\pi^+\pi^-\gamma$ events when the photon is at large angle is described together with the selection efficiency determination and the background evaluation. The two-pion invariant mass spectrum is presented showing a clear signal in the $f_0(980)$ mass region. A corresponding signal is also observed in the profile of the charge asymmetry as function of the invariant mass.

1 Introduction

The scalar isoscalar meson $f_0(980)$ is accessible at KLOE through the electric dipole radiative decay $\phi \to f_0(980)\gamma$. The rate and the f_0 mass distribution of this decay are strictly related to the nature of this scalar particle.

The decay is characterised by the small mass difference between the ϕ meson (1020 MeV) and the $f_0(980)$. Moreover the 2 $K\overline{K}$ thresholds (2M($K^{\pm}$)=987.35 MeV and 2M(K^0)=995.34 MeV) lie between these two masses. The closeness of the masses and the position of the $K\overline{K}$ thresholds, strongly affect the expected f_0 mass spectrum. Since the $f_0(980)\to K\overline{K}$ decays are kinematically suppressed, the final states to look at are the fully neutral $\pi^0\pi^0\gamma$ and the $\pi^+\pi^-\gamma$.

KLOE has already published a study of $\pi^0\pi^0\gamma$ final states [1] based on 17 pb^{-1} of the 2000 data sample, where the f_0 signal is observed and analysed in the M($\pi^0\pi^0$) mass spectrum. The analysis of $\pi^+\pi^-\gamma$ final states requires much more statistics because several unreducible backgrounds with larger rates respect to the signal are present. These backgrounds are essentially the Initial State Radiation (ISR in the following) characterised by the radiative return on the ρ^0, and the Final State Radiation (FSR). The signal of the f_0 has to be searched as a deviation from the expected background shape.

In this memo we present the invariant mass m($\pi\pi$) spectrum and the charge asymmetry profile resulting from the selection of $\pi^+\pi^-\gamma$ final states with the photon at large angle, based on about 350 pb^{-1} taken during 2001 and 2002.

2 Event selection

The events are selected starting from the *drc* stream. The selection chain is the following.

(1) One vertex is required with two opposite charge tracks in the region $R_v < 8$ cm and $|Z_v| < 10$ cm (R_v and Z_v are the radial and longitudinal vertex coordinates).
(2) The two tracks are required to be at "large angle", $45^o < \theta_{tr} < 135^o$.
(3) Each track is extrapolated to the calorimeter and is required to be connected to a cluster; the so called *likelihood* variable L [2] is evaluated for each track and is used to reject $e^+e^-\gamma$ events.
(4) A cut in the so called *track mass* variable M_T ($129 < M_T < 149$ MeV) is applied; it corresponds to the requirement of two pions and a zero-mass third body.
(5) The direction of the missing momentum of the two pion system is required to point in the polar angle region $45^o < \theta < 135^o$. This cut reduces the contribution of the ISR with a limited loss of the signal.
(6) A neutral cluster in the calorimeter is required matching the missing momentum direction. The matching is done cutting on the angle Ω between the photon flight direction and the direction of the missing momentum.

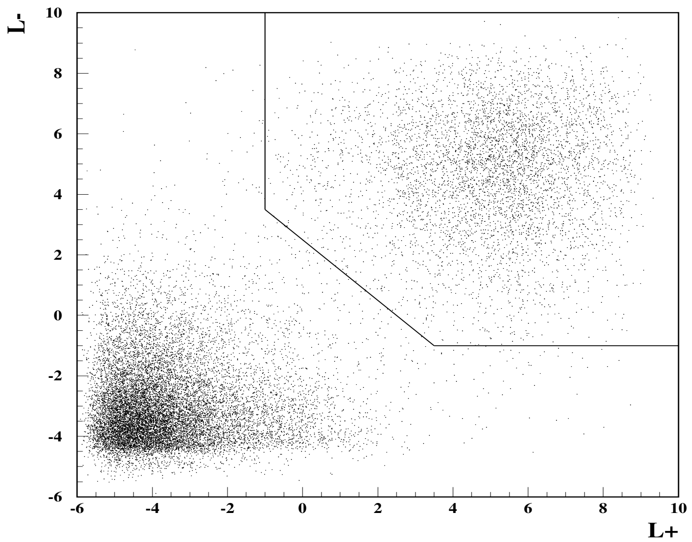

Fig. 1. Scatter plot of L_+ vs L_- for a data sample after cuts (1) and (2). L_+ (L_-) is the likelihood variable for positive (negative) tracks. The line is the cut applied to select between pions (above) and electrons (below) pairs.

The likelihood L is based on the calorimeter information on energy releases and time of flight. Fig. 1 shows the likelihood L_+ for the positive track versus the likelihood L_- for the negative one, for a typical data sample. The two populations correspond to pions and muons (above the cut) and electrons (below the cut).

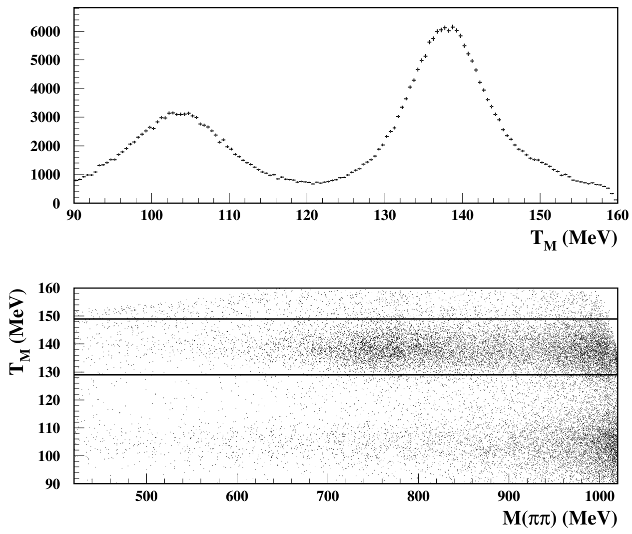

Fig. 2. Distribution of M_T (upper plot) for a data sample after cuts (1) (2) and (3). M_T as a function of the invariant mass M($\pi^+\pi^-$) of the two pions is shown below. Cut (4) is shown in the second plot.

M_T is the mass value that satisfies the equation:

$$|\vec{p}_\phi - \vec{p}_1 - \vec{p}_2| = E_\phi - \sqrt{p_1^2 + M_T^2} - \sqrt{p_2^2 + M_T^2} \tag{1}$$

where $\vec{p}_1$ and $\vec{p}_2$ are the three-momenta of the two pions, E_ϕ and $\vec{p}_\phi$ are the total centre of mass energy and the ϕ boost respectively. Fig. 2 shows the distribution of M_T and the scatter plot of M_T as a function of the invariant mass of the two pions. In the upper plot two separate peaks are visible: one is centred around the muon mass (due to $\mu^+\mu^-\gamma$ events) and one around the pion mass (the $\pi^+\pi^-\gamma$ events). The tail on the right of the pion peak is due to $\pi^+\pi^-\pi^0$ events.

Ω is the 3-d angle between the missing momentum $\vec{p}_{miss}$ and the photon flight direction measured by the cluster position $\vec{p}_\gamma$:

$$\Omega = \frac{\vec{p}_{miss} \cdot \vec{p}_\gamma}{|\vec{p}_{miss}||\vec{p}_\gamma|} \tag{2}$$

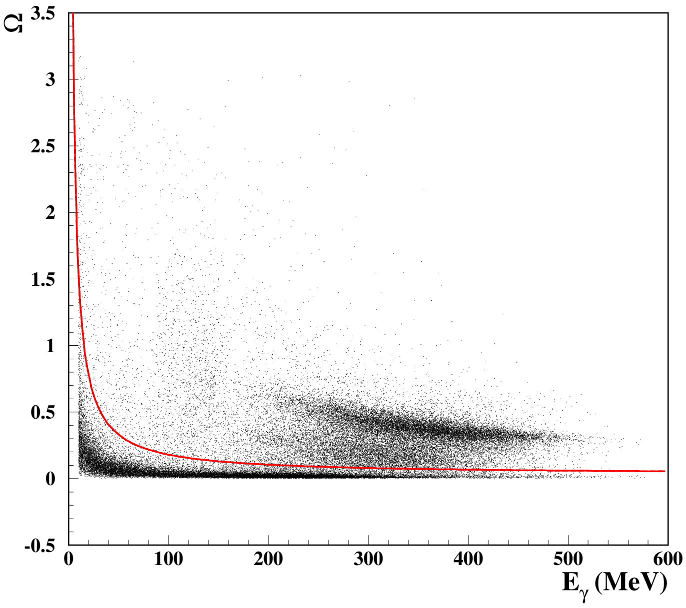

Fig. 3. Angle Ω as a function of the photon energy. The cut is shown. The events above the cut are mostly residual $\pi^+\pi^-\pi^0$ events.

The cut on Ω is a function of the photon energy as shown in Fig. 3. The rejected events in the region $E_\gamma > 200$ MeV, are essentially $\pi^+\pi^-\pi^0$ events, surviving the cut (4). Fig 4 shows the distribution of M_T after cut (6).

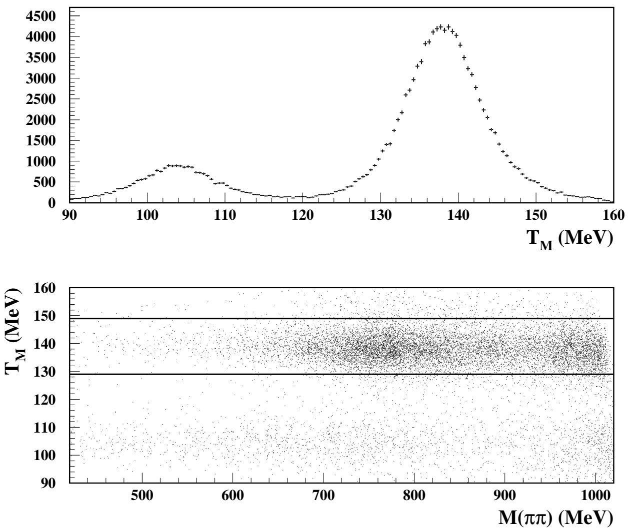

Fig. 4. M_T distribution and T_M vs M($\pi^+\pi^-$) after cut (6) with cut (4) released. The band due to $\pi^+\pi^-\pi^0$ is significantly reduced.

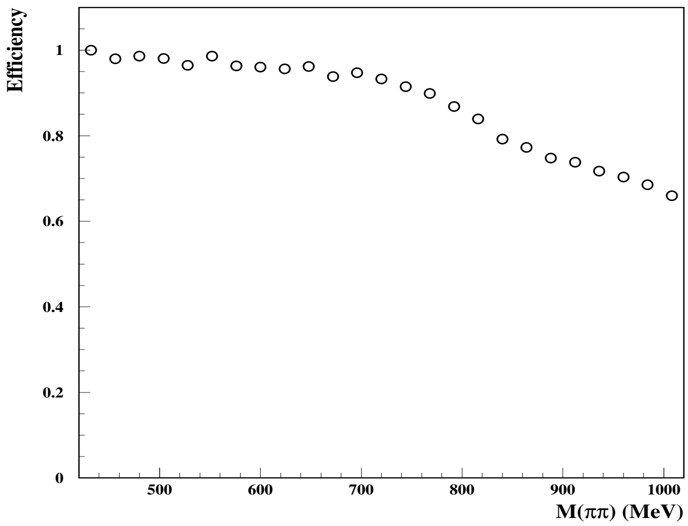

Fig. 5. Veto cosmic efficiency as a function of M($\pi^+\pi^-$). The curve is based on the comparison between the data sample and the pre-scaled events sample.

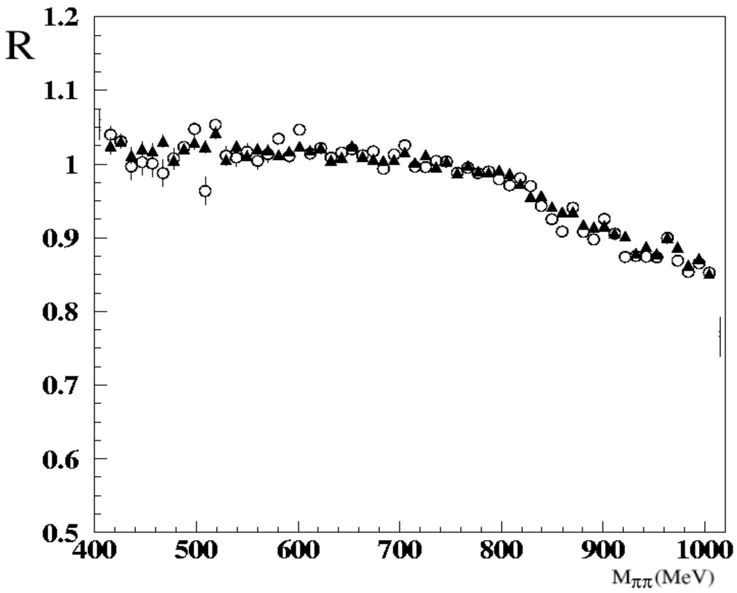

Fig. 6. Ratio between the efficiency of the cosmic veto for data and Montecarlo as a function of M($\pi^+\pi^-$). The circles correspond to 2001 data and the triangles to 2002 data.

3 Selection efficiency

The Montecarlo Geanfi stream *ppphvlag* is used for the evaluation of the efficiency. In this stream Initial and Final State Radiation are simulated [1]. The

[1] The M($\pi^+\pi^-$) shape is simulated according to EVA including collinear radiation.

efficiency is evaluated applying the selection procedure to a Montecarlo sample and looking at the number of surviving events respect to the number of generated events as a function of M($\pi^+\pi^-$). The following cuts have not been applied to the simulated data, the efficiencies for these cuts being obtained from data control samples.

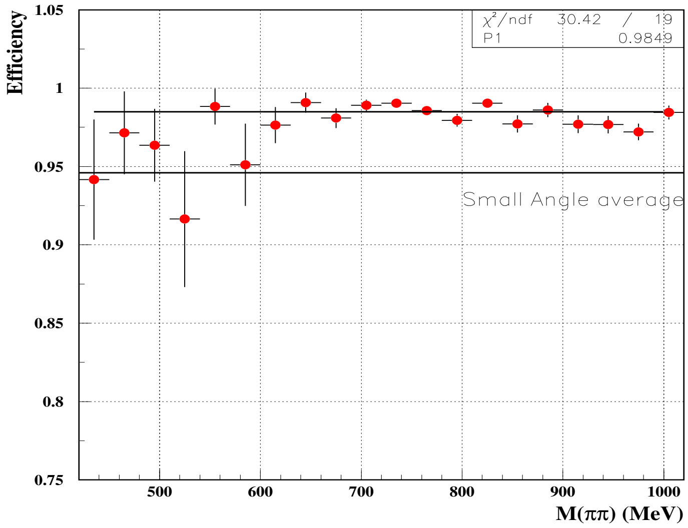

Fig. 7. Efficiency of the *filfo* filter as a function of M($\pi^+\pi^-$). The average value found is compared with the one found in the "small angle analysis".

- The effect of the cosmic veto of the trigger is evaluated looking at the prescaled events, see Fig. 5. Fig.6 shows that the Montecarlo doesn't reproduce correctly the behaviour of this efficiency. It shows also the agreement between 2001 and 2002 data samples.
- The effect of the *filfo* filter is evaluated using samples of data not filtered by *filfo* and looking at the number of events recovered, see Fig 7. Notice that the efficiency loss due to *filfo* is consistently lower than the loss in the "small angle analysis". The small angle topology is more similar to a Bhabha topology (at least according to its definition if *filfo*).
- The efficiency of the procedure to select pions in the calorimeter (association of the track to a cluster and *likelihood* cut) is evaluated using control samples of $\pi^+\pi^-\pi^0$ and is shown in Fig. 8. A small difference between π^+ and π^- efficiencies is observed at low P_t and large angle.

Further corrections to tracking efficiency [3] and low energy photon efficiency are applied weighting the Montecarlo events. For the photon efficiency we have used a data/MC photon efficiency ratio $\sim 1 - e^{-E_\gamma/d}$ ($d = 8.1$ MeV compare with [4]).

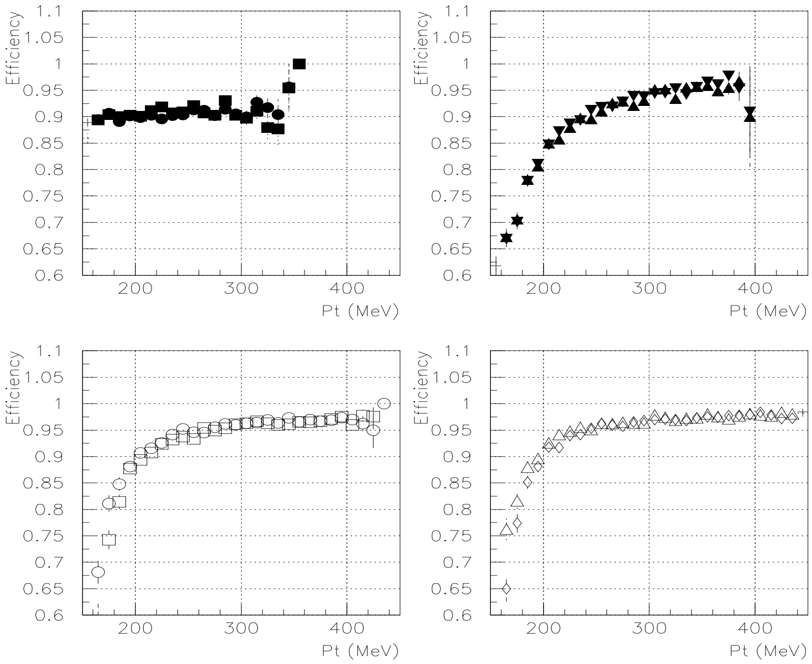

Fig. 8. TCA+Likelihood efficiency as a function of p_t for 4 different angular regions: 40< θ < 50° (upper left); 50< θ < 60° (upper right);60< θ < 70° (lower left); 70< θ < 90° (lower right). The two symbols in each plot refer to π^+ and π^- respectively.

In the higher mass region, corresponding to the low photon energy region, the photon detection efficiency is affected by a systematic uncertainty due to the different data-MC behaviour of the photon energy response close to the 10 MeV energy threshold applied. Fig.9 shows the linearity curves in the low energy region (E_γ < 100 MeV) for data and Montecarlo and the difference between the two. Such a difference results in a systematic uncertainty on the efficiency ranging between 1% and 10% in the points above m=1000 MeV as shown in Fig.9. These systematic differencies are taken as uncertainties and are added in quadrature to the statistical uncertainties in the fit.

The distribution of M_T is characterised by a systematic difference between data and Montecarlo. This is shown in Fig.10. Releasing the M_T cut in a 50 pb^{-1} data sub-sample and applying a double Gaussian fit to the M_T distribution of each M($\pi^+\pi^-$) slice, we obtain average masses and widths for muons and pions. The data Montecarlo comparison shows a significant difference in the pion widths. This difference is taken into account through he efficiency ratio shown in fig.11 that is applied as a weighting function.

The overall efficiency, including all the corrections is shown as a function of M($\pi^+\pi^-$) in Fig.12.

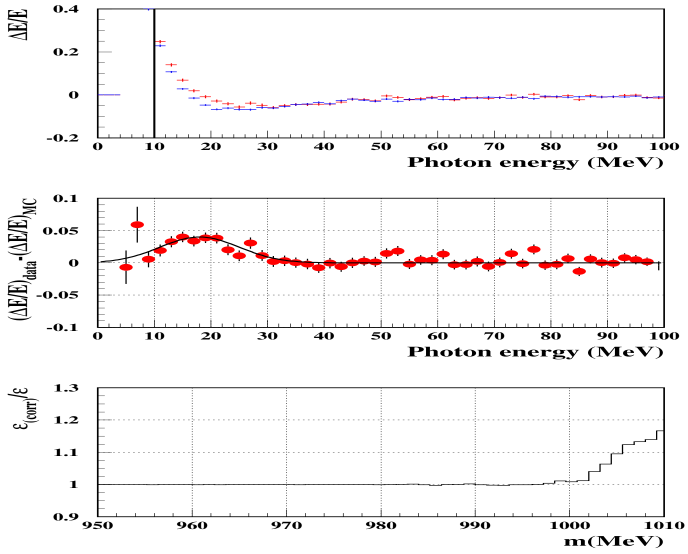

Fig. 9. (First plot) Comparison between the linearity curves from data (red) and Montecarlo (blue) samples. (Second plot) Difference between the two curves. In both cases the photon energy is given by the missing energy of the two charged pions. (Third plot) ratio between the Montecarlo photon efficiency with and without the corrections due to the non-linearity, as a function of m.

A data-MC comparison of the angular distributions of 2001 and 2002 samples in shown Figs.13 and 14. A comparison of the Ω distributions for different slices of M($\pi^+\pi^-$) is also shown (Fig.15).

4 Backgrounds

Possible backgrounds to $\pi^+\pi^-\gamma$ are: $e^+e^-\gamma$, $\mu^+\mu^-\gamma$, $\pi^+\pi^-\pi^0$ and $e^+e^- \to \pi^+\pi^-$ with a very soft photon. Fig.16 shows the normalized prediction of the amounts of each background at the end of the selection procedure, compared to the data spectrum.

$e^+e^-\gamma$ are reduced to a negligible level by the L cut first and then by the M_T cut. $\mu^+\mu^-\gamma$ are rejected by the M_T cut. The M_T resolution for muons (see Fig.10) guarantees that the number of $\mu^+\mu^-\gamma$ events exceeding M_T=129 MeV (the lower acceptance cut in M_T) is negligible (below 0.1% of the signal for all M($\pi^+\pi^-$) spectrum.

$\pi^+\pi^-\pi^0$ events enter in the sample in the low M($\pi^+\pi^-$) region. As a check of the background level, data and Montecarlo expectations have been compared at a previous stage of the analysis, before the requirement of the photon. The m spectrum is strongly affected by $\pi^+\pi^-\pi^0$ events in the low mass region and

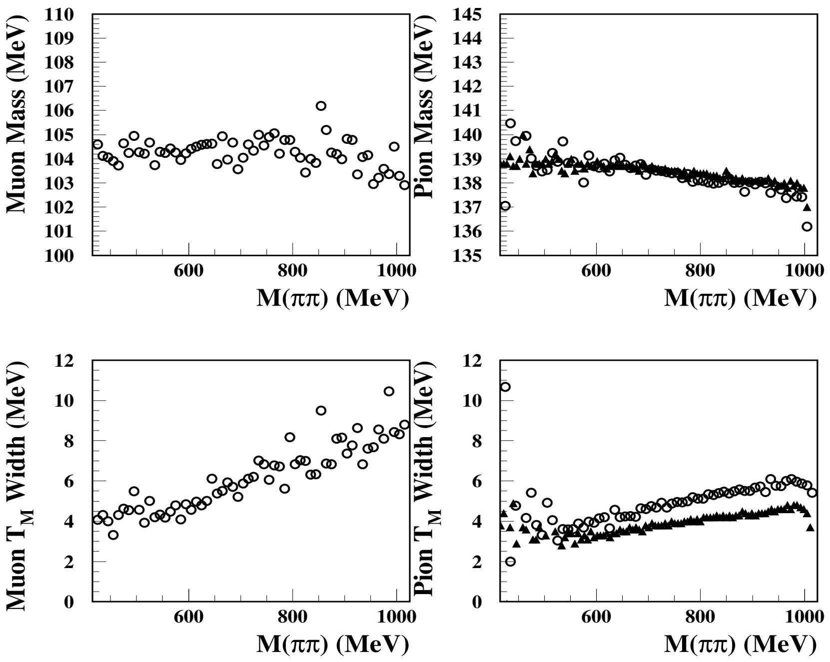

Fig. 10. Average masses and widths from double Gaussian fits of M_T distribution in slices of M($\pi^+\pi^-$). For pions, data (circles) are compared with Montecarlo values (triangles).

by $e^+e^- \to \pi^+\pi^-$ events in the highest mass region. Fig.17 shows for a 40 pb^{-1} data sample, the m spectrum before the request of the photon compared to the spectrum after the photon request normalized by the efficiency for photon detection. The difference between the two spectra is recovered by adding the expected amount of backgrounds at this stage of selection. In order to get a reasonable agreement at least for mass values down to around 450 MeV, the $\pi^+\pi^-\pi^0$ contribution has to be multiplied by 0.47.

5 Invariant mass resolution

The resolution on the invariant mass M($\pi^+\pi^-$) is evaluated using the Montecarlo. Fig. 18(left) shows the distribution of ΔM($\pi^+\pi^-$), the difference between reconstructed and true M($\pi^+\pi^-$). The distribution has a Gaussian shape. The widths and the mean values of ΔM($\pi^+\pi^-$) in different invariant mass ranges are shown in Fig.18(right). No bias in found and the resolution is between 1 and 2 MeV as expected.

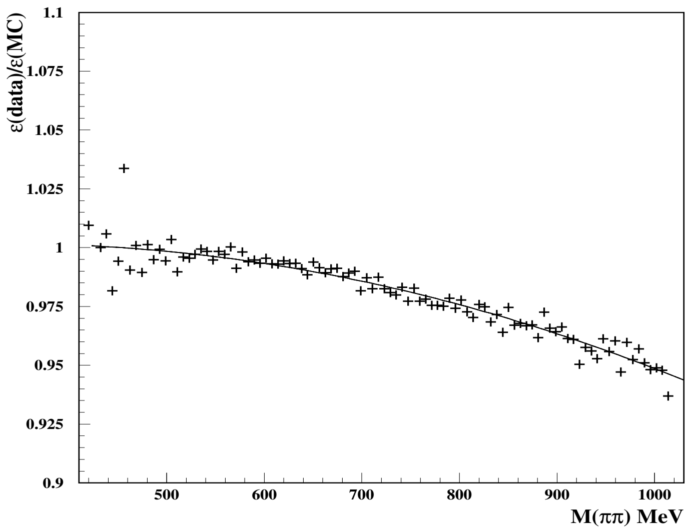

Fig. 11. Ratio of data to MC efficiency for the M_T cut. The curve is used to correct the efficiency.

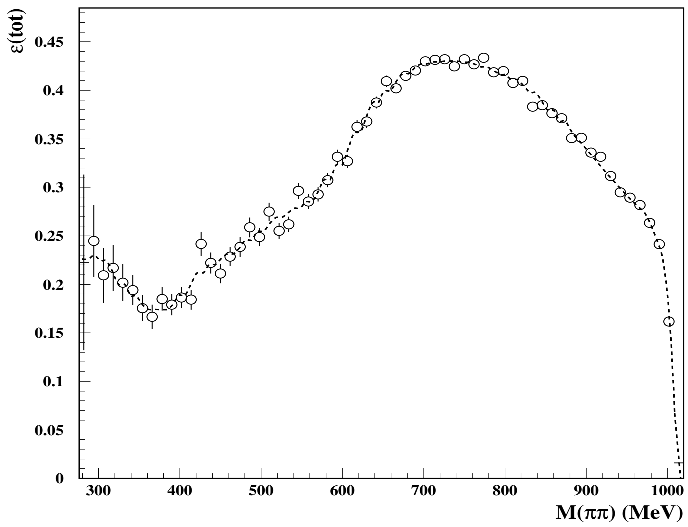

Fig. 12. Total efficiency as a function of M($\pi^+\pi^-$).

6 The invariant mass spectrum

The selection procedure has been applied to a data sample corresponding to 349 pb^{-1} collected in 2001 (115 pb^{-1}) and 2002 (234 pb^{-1}). A final sample of 675590 events is selected. Table 1 shows the number of events and the integrated luminosity in 2001 and 2002. The event rate is consistent between the two samples, the difference being of 0.5%. The signal due to the $f_0(980)$,

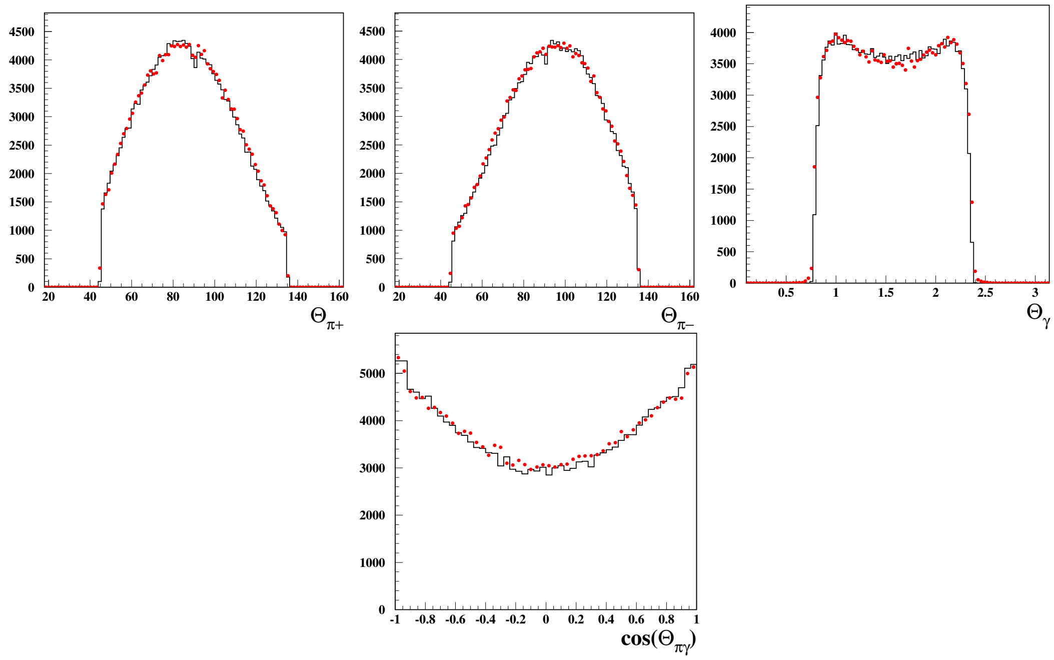

Fig. 13. Comparison of MC (histogram) to data (points) for the 2001 sample; the variables shown are: a) θ_{π^+}, b) θ_{π^-}, c) θ_γ, d) $\cos(\theta_{\pi\gamma})$ (the angle of the photon in the two-pion reference system. The spectra are simply normalised to the number of events.

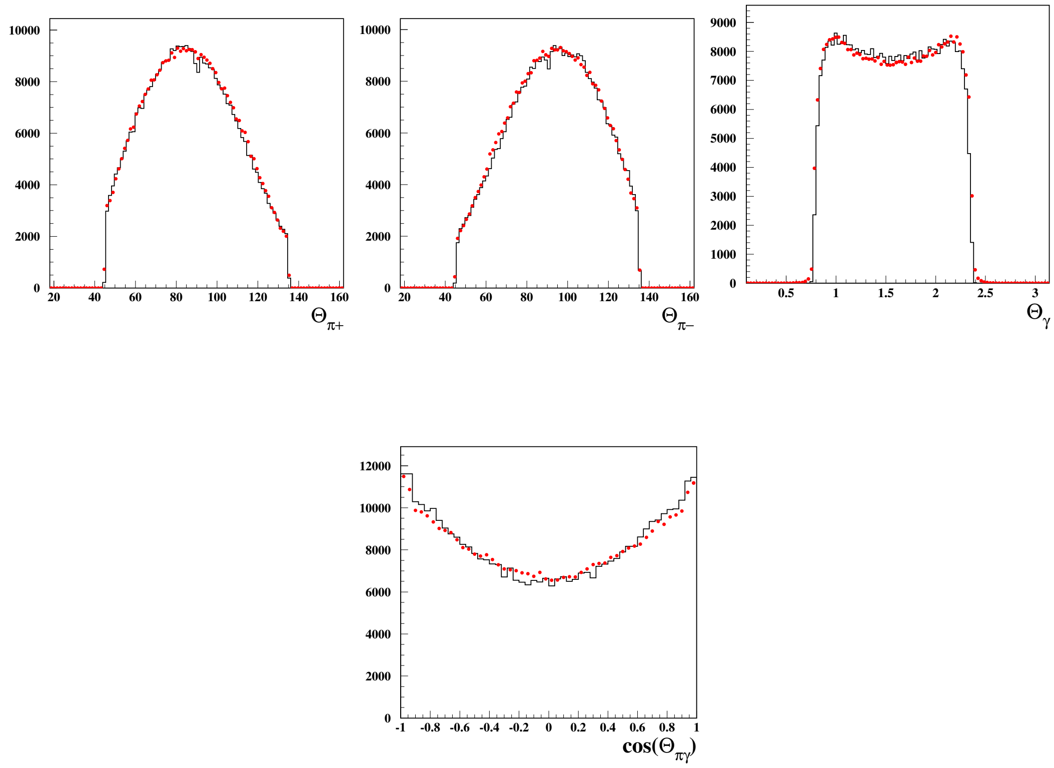

Fig. 14. Same as before for the 2002 sample.

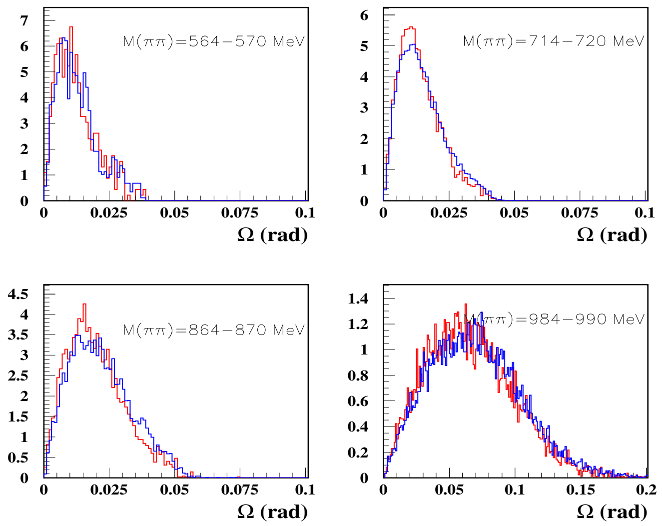

Fig. 15. Data (red) - MC (blue) comparison of Ω distributions in slices of $M(\pi^+\pi^-)$.

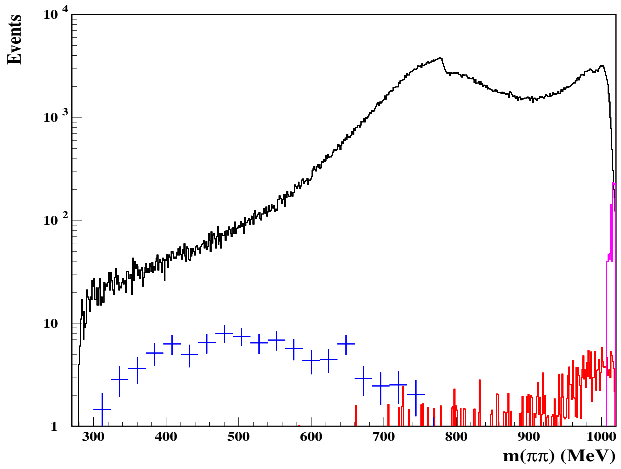

Fig. 16. Data spectrum compared in logarithmic scale to the estimated backgrounds: $\pi^+\pi^-\pi^0$ (blue), $\mu^+\mu^-\gamma$ (red) and $\pi^+\pi^-$ (purple). The backgrounds are normalized according to the total integrated luminosity.

is searched in the invariant mass spectrum of the two pions, $M(\pi^+\pi^-)$, that is defined between $2M(\pi^\pm)$=279.8 MeV and $M(\phi)$=1019.5 MeV. The spectra obtained from the 2001 and the 2002 data samples are shown and compared in Fig. 19 in the full mass range normalised to the integrated luminosity of each sample. In Fig 20 the two spectra are plotted in the invariant mass region from 900 MeV and 1020 MeV where the f_0 signal is present.

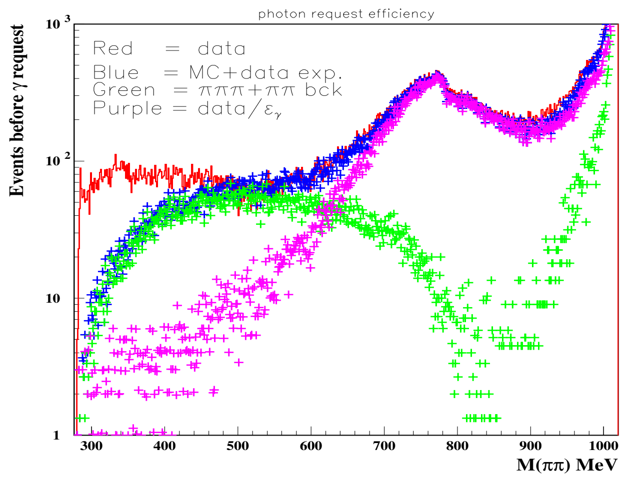

Fig. 17. Data spectrum before the photon request for a 40 pb^{-1} sample (red) compared to the spectrum after the photon request divided by the efficiency for photon detection (purple); expected background at this analysis stage (green) and sum of signal and background at the same analysis stage (blue).

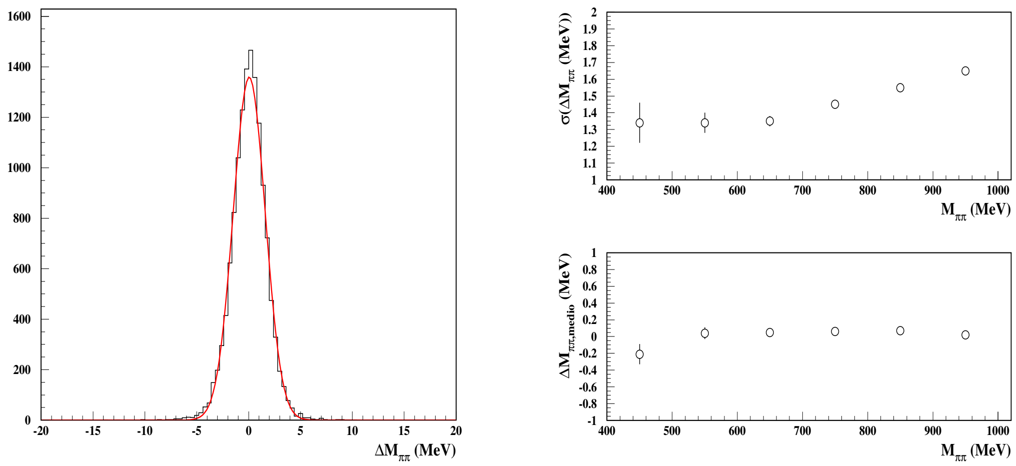

Fig. 18. (left) $\Delta M(\pi^+\pi^-)$. (right) width and mean value of the $\Delta M(\pi^+\pi^-)$ distribution as a function of the invariant mass .

The ρ resonance and the ρ- ω interference dominate the mass region around 770 MeV. The final state radiation together with the low mass tail of the ρ' dominate the region above 850 MeV. The f_0 contribution is visible around 980 MeV. After 1000 MeV a drop is observed due to the efficiency in the detection of photons with energies below the 20 MeV region.

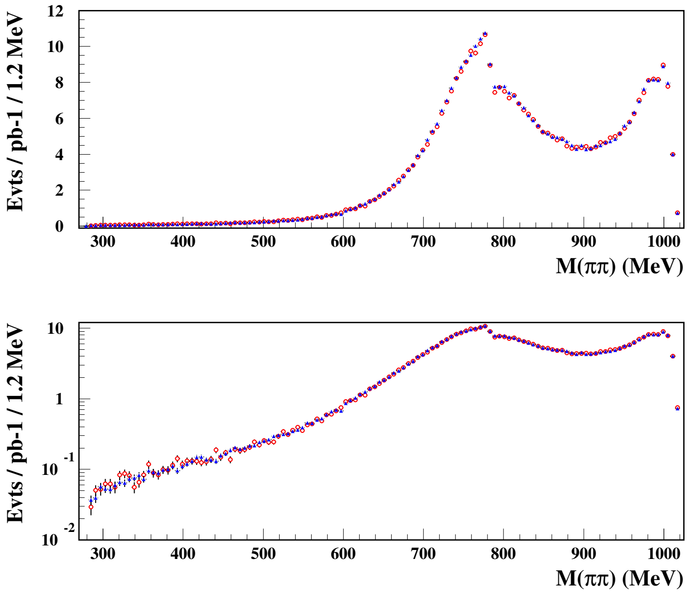

Fig. 19. Comparison between the 2001 (red circles) and 2002 (blue triangles) final invariant mass spectra in bins of 6 MeV in linear and logarithmic scales. The distributions are normalised to the integrated luminosities.

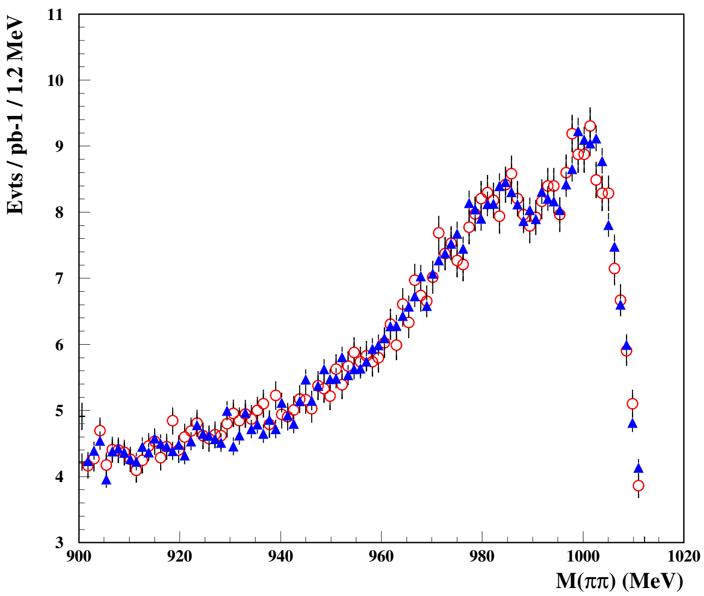

Fig. 20. Same comparison in bins of 1.2 MeV in the mass region between 900 and 1020 MeV. Again the distributions are normalised to the integrated luminosities.

	Number of events	Luminosity (pb^{-1})	$R = N/L$ (evts / $pb^{-}1$)
2001	221178	115	1923
2002	454412	234	1934

Table 1
Number of events, integrated luminosity and event rate for the 2001 and 2002 data samples.

7 The charge asymmetry

The $\pi^+\pi^-$ systems from ISR and from FSR decay have opposite charge conjugation, respectively odd and even. Any interference term between the two amplitudes is odd under charge conjugation and gives rise to a charge asymmetry. The f_0 term gives also a C-even term. We define the charge asymmetry as (θ^+ is the polar angle of π^+):

$$A = \frac{N(\theta^+ > 90^o) - N(\theta^+ < 90^o)}{N(\theta^+ > 90^o) + N(\theta^+ < 90^o)} \tag{3}$$

Fig.21 shows the behaviour of the observed charge asymmetry as a function of $M(\pi^+\pi^-)$ superimposed to the expectation in case of FSR and ISR only based on the EVA Montecarlo. The data follow the expectation except in the region of the f_0 where a narrow structure is observed. This effect indicates that a C-odd interference term between the f_0 and the ISR is present with opposite sign respect to the one between FSR and ISR. It is also a largely independent indication of the f_0 signal. Notice that below 700 MeV Montecarlo rises up to a plateau of ~ 0.15 while data are around 0. This is another discrepancy not understood.

8 Conclusion

We have observaed a clear signal in the $\pi^+\pi^-$ invariant mass spectrum and in the charge asymmetry dependence on the invariant mass. The signal is in the region of the f_0.

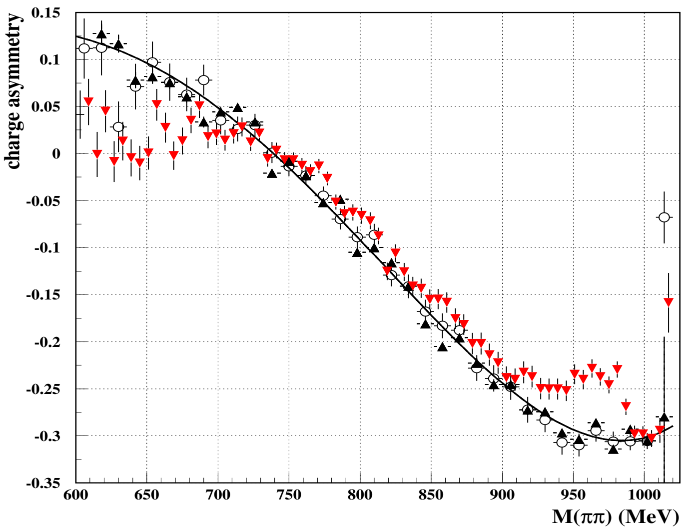

Fig. 21. Charge asymmetry vs. M($\pi^+\pi^-$). Montecarlo expectation based on generated variables (open circles), based on reconstructed variables (upward triangles) and data (red downward triangles).

In a forthcoming note fits to the data will be shown.

References

[1] KLOE collaboration 'Study of the decay $\phi \to \pi^0\pi^0\gamma$ with the Kloe detector', Phys. Lett. B537 (2002);

[2] B. Valeriani KLOE Memo 295, July 2004;

[3] M.Incagli, talk given at Capri KPW03;

[4] M.Palutan, T.Spadaro and P.Valente, KLOE Note 174 (2002);